Two-dimensional threshold-based cloud-type classification using MTSAT data

DWI PRABOWO YUGA SUSENO*†, TOMOHITO J. YAMADA†
† Graduate School of Engineering, Hokkaido University, Sapporo 060-8628, JAPAN
* Corresponding author; Email: dwiprab@eng.hokudai.ac.jp

A new two-dimensional threshold diagram (2D-THR) has been developed based on maximum likelihood cloud classification results, which can readily be applied for Multi-functional Transport Satellite (MTSAT) split window datasets. Since 2D-THR was trained using northern summer 2010 data for Japan and its surrounding area, it is typically suitable only for summer. Comparison of snapshot cloud-type distributions showed that 2D-THR images and the corresponding night-time microphysical colour composite images as well as 2D-THR and Japan Meteorological Agency (JMA) cloud-type images are in good agreement. A time series inter-comparison of the hourly 2D-THR cloud classification results with the JMA cloud type classification data product was performed by calculating spatial correlation of cloud percentage for 1° × 1° grid cells. For cumulonimbus, high-level, middle-level, and low-level clouds over tropical and subtropical areas in the northwestern Pacific Ocean region, the spatial correlation between 2D-THR and JMA is moderate. Thus, 2D-THR cloud-classification algorithm can be applied in both regions.

1. Introduction

Accurate and automatic satellite-based cloud detection and classification is useful for numerous climatic, hydrologic and atmospheric applications (Liu *et al.* 2009). Cloud-type information is necessary for practical applications, such as indirect rainfall estimation by using an infrared (IR) channel (centred at 10.8 μm). This is because in the indirect rainfall estimation method, lower cloud top temperature, as depicted in IR images, is assumed to be associated with heavy rainfall. This assumption is suitable for convective clouds, but not so for nonconvective clouds (Kuligowski 2003). In this situation, cloud-type information helps distinguish convective clouds such as cumulonimbus (Cb) from other cloud types, such as cirrus (Ci), which have low temperatures but do not produce rain.

The Cloud-type classification methods can be categorized into supervised classification and unsupervised classification methods. The term “supervised” indicates that the analyst can control the categories or classes according to their specific purposes. Classification algorithms such as the maximum likelihood algorithm (Bolle 1985) and neural networks (Shi *et al.* 2005) are usually employed in the supervised classification method. However, this method is relatively labour intensive, especially during training area selection. Unsupervised classification, which employs simple processes, such as a threshold technique, is most commonly used for cloud-type classification (Liu *et al.* 2009). Some threshold algorithms that are based on multispectral satellite images combined with ancillary information such as weather prediction or observation (e.g.

rawinsonde) have been developed (Inoue 1987, Feidas *et al.* 2000). The additional information helps define thresholds for classifying the satellite images on the basis of vertical temperature profiles of the atmosphere. However, these algorithms have limitations when they are applied to regions for which such supporting information is not available.

This study has two objectives. The first objective is to develop new threshold-based cloud-type classification algorithm in which only the split window channel datasets of Multi-functional Transport Satellite (MTSAT) are employed. We intend to use low-cost computational systems to develop a simple algorithm that can be implemented in regions for which weather information is not available. The second objective is to validate the new threshold algorithm spatially as well as temporally by comparing it with other cloud classification data products.

2. Study Area and Data

The domain for developing the new threshold cloud-type classification covers Japan and its surrounding area (30°N–50°N and 120°E–150°E). The validation area covers northwestern Pacific Ocean (0°–52° N and 114° E–160° E). The validation area was larger than the development area because we considered examining the possibility of applying the new threshold in a tropical region. We acquired MTSAT images for the northern summer i.e. June, July, August, and September (hereafter JJAS) for 2009 and 2010. The images used are freely downloadable from the websites of Institute of Industrial Science, University of Tokyo (Takeuchi *et al.* 2010) and Kochi University Weather Home (Kochi University 2011). MTSAT 2R has been operational since 1st July 2010 and it has replaced MTSAT 1. Consequently, we utilized MTSAT 1 for JJAS 2009 and June 2010 and MTSAT 2R for July to September 2010. However, due to the same specifications of visible and IR sensors for both MTSAT 1 and 2R, we assume that there is no difference in the spectral characteristics of the images. In the study region, the spatial resolution of MTSAT data is ~5 × ~5 km. Moreover, MTSAT has a temporal resolution of 1 h and has five spectral channels that are centred at 0.725 μm (Visible), 10.8 μm (IR1), 12.0 μm (IR2), 6.75 μm (IR3), and 3.75 μm (IR4).

The Japan Meteorological Agency cloud-type classification data product (hereafter JMA) was utilized for the inter-comparison. The spatial and temporal resolutions of the JMA are 0.25° × 0.25° (~25 km × ~25 km) and 1 h, respectively. JMA uses MTSAT images as well as additional information in their cloud type classification algorithm. There are two main processing steps for classifying the raw image pixel, namely stratification and discrimination. In the first step, a dynamic threshold is employed to slice the IR1 image by using the vertical temperature profile of the atmosphere at 400-hPa and 600-hPa levels; the temperature profile is derived from meteorological reanalysis data. In the second step, for the determination of more specific cloud type, especially for the lower level clouds, the reflectance information from visible and IR brightness temperatures as well as IR channel difference, for example, IR1 - IR2 and IR1 - IR3, has been employed (JMA 2007).

3. Method and Results

We developed a threshold boundary for cloud type classes; this boundary was represented in a two-dimensional threshold diagram (hereafter 2D-THR) of IR1

brightness temperature (T_{IR1}) vs. the brightness temperature difference between IR1 and IR2 ($\Delta T_{IR1\text{-}IR2}$). Here, we used the results of supervised cloud-type classification to adjust the threshold boundary among cloud types. The cloud type clusters derived from the supervised cloud-type classification then were plotted by using their mean centres in a T_{IR1} vs. $\Delta T_{IR1\text{-}IR2}$ scatterplot.

The development of new a threshold began with selecting images that were used for cloud-type analysis by supervised multispectral classification. Eight classes were considered for cloud-type analysis in this study. These were Cb, mature Cb (MCb), thick cirrus (TkCi), thin cirrus (TiCi), middle-level cloud (MC), low-level cloud (LC), clear land area, and clear sea area. Images that clearly depicted these cloud classes were selected. We selected 41 scenes of images as a representation of each month during the JJAS 2010 period. Of these, 11, 9, 11, and 10 scenes represented June, July, August, and September, respectively. We assumed that since the images for JJAS 2010 were used, the resulting threshold diagram would be valid specifically for the summer season.

A false colour image composite called Night Microphysical colour scheme (Lensky and Rosenfeld 2008) was used as the background image for identification of the cloud types during training area selection. We also considered some visual cloud properties such as texture, organizational pattern, edge definition, size, and individual shape (Conway 1997).

We adopted two types of image classification algorithms, namely, maximum likelihood (hereafter MAX) and multilayer perceptron neural network (hereafter NN) for multispectral supervised classification. The performances of these algorithms were compared by using the same input bands and training sample areas during the classification process.

A map-to-map comparison was conducted to determine the agreement between MAX vs. JMA and NN vs. JMA by using the kappa coefficient of agreement (K_{hat}). $K_{hat} > 0.8$ represents strong agreement; $0.4 < K_{hat} < 0.8$ represents moderate agreement; and $K_{hat} < 0.4$ represents poor agreement (Jensen 2005). A reclassification and resampling procedure helped compare the data in terms of the cloud classes and spatial reference. K_{hat} values were calculated for the 41 pairs of resampled images of MAX vs. JMA cloud-type and NN vs. JMA cloud-type. Figure 1 shows a graphical comparison of the K_{hat} values of these image pairs. The average K_{hat} for MAX vs. JMA cloud type and NN vs. JMA cloud type are 0.44 and 0.42, respectively. These values indicate moderate agreement between the supervised classification result and JMA cloud type. The results confirm that MAX has slightly better agreement than NN; therefore, we decided to use MAX cloud classification results to train the 2D-THR.

On the basis of MAX cloud classification results, we generated cloud-type clusters by plotting the T_{IR1} and $\Delta T_{IR1\text{-}IR2}$ of corresponding cloud types derived from 41 classified images. However, it proved difficult to delineate the border of each cloud-type cluster for defining the threshold boundary value from such cloud-type scatterplots, because of the overlapping of the cloud-type clusters. To overcome this problem, we modified the original scatter diagram by plotting only the mean centre of the cloud cluster, instead of all points. The mean centre of the cloud cluster was calculated for every cloud type by using the equation (Rogerson 2006):

$$X_c = \sum_{i=1}^{n} w_i T_{IR1} \Big/ \sum_{i=1}^{n} w_i ; \quad Y_c = \sum_{i=1}^{n} w_i \Delta T_{IR1\text{-}IR2} \Big/ \sum_{i=1}^{n} w_i \tag{1}$$

where X_c and Y_c are the coordinates of the mean centre of the cluster of cloud-type *c*. Further, w_i is the weight of point *i*, i.e., the position of T_{IR1} and $\Delta T_{IR1\text{-}IR2}$ in the scatterplot, *n* is number of points. The weight was calculated by dividing the frequency of occurrence of point *i* by the total frequency of occurrence of all points. This process can simplify the cloud-type scatterplot distribution because currently it only consists of 41 points representing the mean centres of each cloud type (figure 2(*a*)). Here, the grouping of cloud-type cluster can be more easily evaluated.

An adjustment process was performed by tuning the boundary values of the diagram and comparing the 2D-THR classified images using current threshold values with the corresponding MAX images for the 41 cases. Several iterations of the adjustment process were conducted until at least moderate agreement with most of the MAX images was realized. From 41 comparisons between 2D-THR and MAX images, we got 38 image pairs that satisfied the conditions $K_{hat} > 0.4$. The final 2D-THR threshold boundary is shown in figure 2(b). This 2D-THR can be used as a look-up table by comparing the combination of values of T_{IR1} and $\Delta T_{IR1\text{-}IR2}$ for the same pixel location with the diagram to get the cloud-type image.

Before applying 2D-THR for retrieving the cloud type, we identify the cloud pixels by using the IR1 channel. We followed the cloud-pixels screening relations derived by Choi and Hoi (2009). However, we modified the relations since we utilized only T_{IR} for day and night-time cloud detection by following relations:

$$(T_{IR1}{}^{clr} - T_{IR}) > \delta_{IR} \qquad (2)$$

where $T_{IR1}{}^{clr}$ and T_{IR1} are the IR1 clear-sky brightness temperature and $T_{10.8}$ total-sky brightness temperature, respectively. The IR1 clear-sky value is the maximum value of all IR1 images for August 2010. We applied equation 2 to the previous 41 scenes to get the binary images represent cloudy and non cloudy area. The value of δ_{IR} given by Choi and Hoi (2009) was utilized as the initial value. We tuned the δ_{IR} by visually comparing the cloud binary images with the cloud features depicted by the corresponding night microphysical colour composite images. The adjusted value of δ_{IR} was 20K for detecting cloud over land and 7K over sea. The value was higher than that specified by Choi and Hoi (2009) i.e. 8K for land and 3.5K for sea. It was most probably due to different area of coverage which influenced the value of IR1 clear-sky.

The ideal way of validating the cloud-type classification result is to compare the data with actual weather observations. Owing to the lack of observation data, we compared 2D-THR with the JMA product. Since both data sets are basically the result of estimation with their own uncertainty, in this case we simply compare the geographical relationship of cloud-type occurrence represented by both data sets. We utilized spatial correlation to show such spatial relationships between 2D-THR and JMA cloud classification. Within a 1° × 1° grid cell for respective 2D-THR and JMA images, the number of pixels for every cloud type was counted. We preserved the original resolution of both corresponding cloud classifications during this process. The cloud-type percentage was calculated for each grid cell by dividing the count of number of cloud types by the total number of cloud pixels within the grid area. Thus, a cloud percentage map was generated from 2D-THR and JMA images for each cloud type, and we calculated the correlation coefficient accordingly (Rogerson 2006). However, since 2D-THR is based on a split window channel, it has limitations when a more detailed classification scheme such as that in JMA is used. Hence, 2D-THR uses a simpler

cloud-type classification than JMA. Therefore, we have to reclassify the classification scheme of 2D-THR and JMA for them to be comparable with the new classifications shown in table 1. TiCi and TkCi in the 2D-THR classification scheme were reclassified as high-level cloud (HC), thus Stratocumulus, Cumulus, Stratus/Fog in the JMA classification scheme were reclassified as LC in the new reclassified classes.

Table 1. Reclassification of 2D-THR and JMA cloud-type classifications

2D-THR	JMA	New reclassified classes
Clear (land and sea)	Clear	Clear
Cb	Cb	Cb
MCb	Dense Cloud	HC
TiCi, TkCi	HC	HC
MC	MC	MC
LC	Stratocumulus, Cumulus, Stratus/Fog	LC

4. Discussion

Several uncertainties associated with the adjustment process of 2D-THR threshold boundary probably influence the accuracy of the cloud-type classification result. Some mean centres of certain classes are omitted because they are included in the adjacent class; this has been observed in the case of the area around 225 K < T_{IR1} < 230 K and $\Delta T_{IR1\text{-}IR2}$ < -0.5 K; 225 K < T_{IR1} < 230 K and 0.5 K < $\Delta T_{IR1\text{-}IR2}$ < 1.5 K; and 275 K < T_{IR1} < 280 K and 1 K < $\Delta T_{IR1\text{-}IR2}$ < 2 K. The same adjustment process was also performed to adjust the area which lack of mean centre of cloud type such as the area corresponding to 290 K < T_{IR1} < 295 K and 0 K <$\Delta T_{IR1\text{-}IR2}$ < 1.5 K, and 245 K < T_{IR1} < 255 K and -0.5 K < $\Delta T_{IR1\text{-}IR2}$ < 0 K. For the outer boundary of the 2D-THR, extrapolation was based on the outer boundary cluster of cloudy pixels in the T_{IR1} and $\Delta T_{IR1\text{-}IR2}$ scatterplot. Another uncertainty also should be notified, in terms of defining the cloudy pixels according to Choi and Hoi (2009) where the modification of δ_{IR} was intended to somewhat reduce the distribution of some fraction of clouds for several image cases especially LC.

A snapshot of the cloud-type classification results obtained using the 2D-THR algorithm for 2 August 2009 at 02:30 UTC is shown in figure 3(*a*), along with the corresponding night-time microphysical colour composite image (figure 3(*b*)). We can see in figure 3(*b*), Cb and MCb that respectively shown in red and dark orange are accurately portrayed in the cloud-type classification image (figure 3(*a*)). The distribution of TiCi and TkCi depicted in dark blue and violet as well as MC represented in yellow to orange also reasonably match with cloud-type image. However, LC shown in pale pink seems to be partially portrayed in the cloud-type image.

Figure 4 shows the inter-comparison between 2D-THR and JMA cloud type images for the same period as in figure 3. However, 2D-THR is resampled into the same spatial resolution as JMA and both are reclassified according to the same cloud classes as shown in table 1. We can see that 2D-THR shows a larger cloud distribution area for Cb and a smaller cloud distribution area for LC than JMA. However, for HC and MC, the cloud distribution areas seem comparable.

The time series inter-comparison of hourly 2D-THR images and the JMA cloud classification was also performed for the JJAS 2009 period by comparing the spatial correlation of cloud-type percentage. Since the 2D-THR is developed for the northern summer in subtropical regions, we examine the possibility of applying this method to tropical regions. Therefore, we divide the validation area into tropical and subtropical regions and compare the validation results accordingly. The spatial correlation of cloud-type percentage was calculated after completing the reclassification and aggregation processes. The calculation results of tropical region shows that the average values of the spatial correlation are moderate, i.e. 0.64, 0.56, 0.47, and 0.55 for Cb, HC, MC, and LC, respectively. Similar moderate spatial correlations are also seen for subtropical regions, i.e. 0.54, 0.71, 0.55, and 0.59 for Cb, HC, MC, and LC, respectively. Since the spatial correlation expressed the geographical relationship of the frequency of occurrence of the cloud type, these results demonstrate that the distribution of cloud type represented by 2D-THR is reasonably comparable for tropical and subtropical regions. This suggests that 2D-THR can be applied in both areas.

Figure 5 shows the hourly variations in the spatial correlations of Cb, HC, MC, and LC cloud percentage for tropical and subtropical regions. As already mentioned in section 3, during the calculation of cloud percentage, we preserve the original resolution of 2D-THR and JMA. Since 2D-THR has higher spatial resolution than JMA, it can represent local or isolated cloud better than JMA. This means that for certain times, 2D-THR and JMA representations of local or isolated clouds may differ. This is probably a contributing factor to the very high fluctuation of spatial correlation of cloud percentage as is observed for all cloud types in mid-July and in September. We observe that the spatial correlation in both tropical and subtropical regions is strongly influenced by a diurnal pattern of cloud percentage such as that clearly shown by HC, MC and LC in both tropical and subtropical regions. Detailed inspection of the figures demonstrates that the variation in diurnal patterns among cloud types sometimes has the opposite pattern because of the multi-layer effect of clouds. When the cloud percentage of a higher level cloud increases, it reduces the cloud percentage of the lower level cloud since the higher level cloud blocks the lower cloud level; therefore, the spatial correlation tends to decrease.

5. Conclusions

A new 2D-THR cloud-classification algorithm has been developed; it was trained using MAX classification results for Japan and its surrounding area. The cloud-type classification boundary was defined by adjusting the threshold value of the distribution of mean centre of the cloud-type clusters in the T_{IR1} and $\Delta T_{IR1\text{-}IR2}$ scatter diagram. Images for northern summer (JJAS) 2009 were used for developing the 2D-THR; therefore, this diagram is typically suitable for classifying clouds during the summer. During the adjustment process, the mean centres of certain classes were omitted because they were included in an adjacent class. This may be considered as the main uncertainty of this method. The presence of some areas in the 2D-THR that lack of mean centres of cloud clusters suggests that 2D-THR should be trained by using more MAX images.

However, visual inter-comparison of a snapshot image for 2 August 2009 02:30 UTC between a 2D-THR image and its corresponding night-time microphysical colour composite image, shows that most of cloud types identified in the colour composite

image were well represented in the2D-THR image. Inter-comparison of the JMA image and 2D-THR for the same period also proves good visual agreement between the two.

The cloud percentages for JMA and 2D-THR during JJAS 2009 over tropical and subtropical regions were spatially correlated. The results showed that the geographical distribution of the frequency of occurrence of each cloud type is moderately represented by 2D-THR. It suggests that 2D-THR can be reasonably applied for tropical and subtropical regions. 2D-THR has higher spatial resolution than JMA; hence, it can represent local or isolated cloud better than JMA. However, its cloud-type representation is different. The graphical comparison of the spatial correlation of cloud percentage during JJAS 2009 demonstrates very high fluctuation of spatial correlation for certain times; this fluctuation is most probably caused by different representations of the local cloud type. The graph also showed opposite patterns of diurnal variation among the cloud types because of a multilayer cloud effect.

Acknowledgements

The authors wish to express their gratitude to Dr. Yadu Pokhrel for helpful comments and suggestions. This study was partially supported by the Integrated Study Project on Hydro-Meteorological Prediction and Adaptation to Climate Change in Thailand (IMPAC-T), Science and Technology Research Partnership for Sustainable Development, JST-JICA, Japan, and Research Program on Climate Change Adaptation, Ministry of Education, Culture, Sports, Science and Technology (RECCA/MEXT). The anonymous reviewers and the editor of this journal are deeply thanked for their valuable and very helpful comments.

References

BOLLE, H. J., 1985, Validation of thin cirrus and low cloud cover over snow by means of maximum likelihood method. *Advance Space Research*, **5**, pp. 169–175.

CHOI, Y.-S., and HOI, H.C., 2009, Validation of cloud property retrievals from MTSAT-1R imagery using MODIS observations. *International Journal of Remote Sensing*, **30,** pp. 5935–5958.

CONWAY, E. D., 1997, *An introduction to satellite image interpretation*, pp. 1–242 (Maryland: The John Hopkins University Press)

FEIDAS, H. N., C. CARTALIS, A.P. CRACKNELL, 2000, Use of Meteosat imagery to define clouds linked with floods in Greece. *International Journal of Remote Sensing*, **21**, pp. 1047–1072.

INOUE, T., 1987, An instantaneous delineation of convective rainfall areas using split window data of NOAA-7. *Japan of Meteorological Society*, **65**, pp. 469–480.

JENSEN, J. R., 2005, *Introductory Digital Image Processing: a remote sensing perspective*, pp. 1 - 526 (New Jersey: Pearson Prentice Hall).

JMA, 2007, Information about the use of the northwestern Pacific Ocean cloud cover grid point (in Japanese). Japan Meteorological Agency

KOCHI UNIVERSITY, 2011, GMS/GOES9/MTSAT Data Archive for Research and Education. Available online at: http://weather.is.kochi-u.ac.jp/archive-e.html (accessed August 2011).

KULIGOWSKI, J., 2003, Remote Sensing in Hydrology. Available online at: http://www.weather.gov/iao/InternationalHydrologyCourseCD1/1029/wmo_bk.ppt (accessed 4 November 2007).

LENSKY, I. M., and ROSENFELD, D., 2008, Clouds-Aerosols-Precipitation Satellite Analysis Tool (CAPSAT). *Atmospheric Chemistry and Physics*, **8**, pp. 6739–6753.

LIU, Y., XIA, J., SHI, C. X., and HONG, Y., 2009, An improved cloud classification algorithm for China's FY-2C multi-channel images using artificial neural network, *Sensor*, **9**, pp. 5558–5579.

ROGERSON, P. A., 2006, *Statistical Method for Geography*, pp. 1 - 304 (Los Angeles: SAGE Publications)

SHI, C., WENJIAN, Z., WEI, G., and LIYANG, Z., 2005, Study on cloud classifications by using AVHRR, GMS-5 and Terra/MODIS satellite data. Available online at: http://cimss.ssec.wisc.edu/itwg/itsc14/proceedings/A06_shi.pdf (Accessed 25 Jan 2011)

TAKEUCHI W., NEMOTO, T., KANEKO, T. AND YASUOKA, T., 2010. Development of MTSAT data processing, distribution and visualization system on WWW. *Asian Journal of Geoinformatics*, **10**, pp. 29–33.

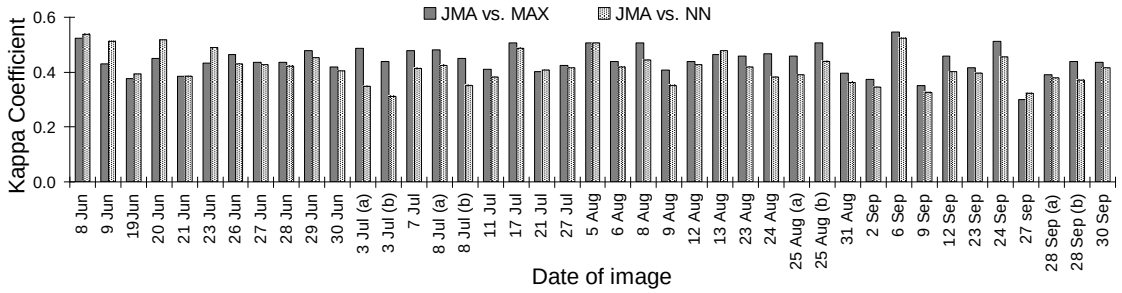

Figure 1. Comparison of K_{hat} values between JMA vs. MAX and JMA vs. NN for selected images during JJAS 2010.

(*a*) (*b*)

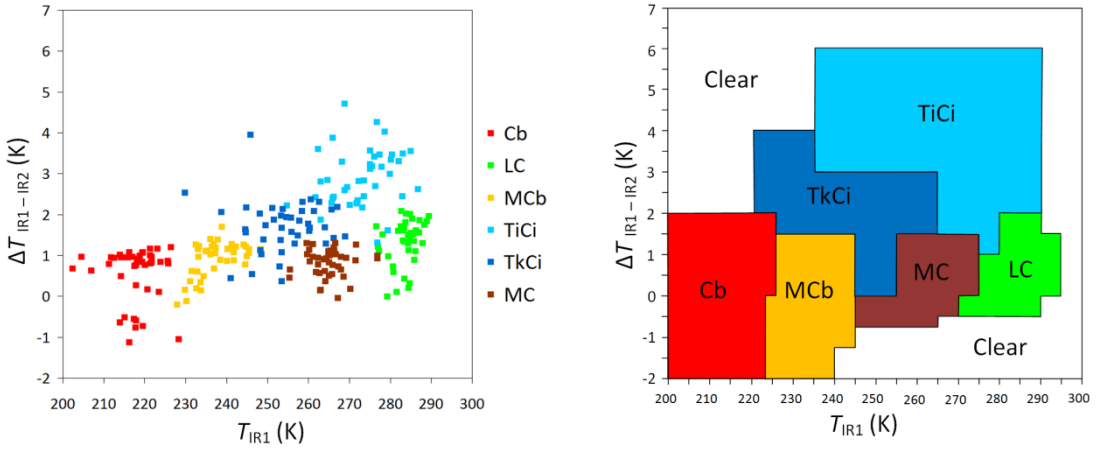

Figure 2. (*a*) A scatter plot of mean centre of each cloud type derived from MAX classification results; (*b*) 2D-THR for cloud-type classification by using T_{IR1} and $\Delta T_{IR1\text{-}IR2}$ of MTSAT 1R.

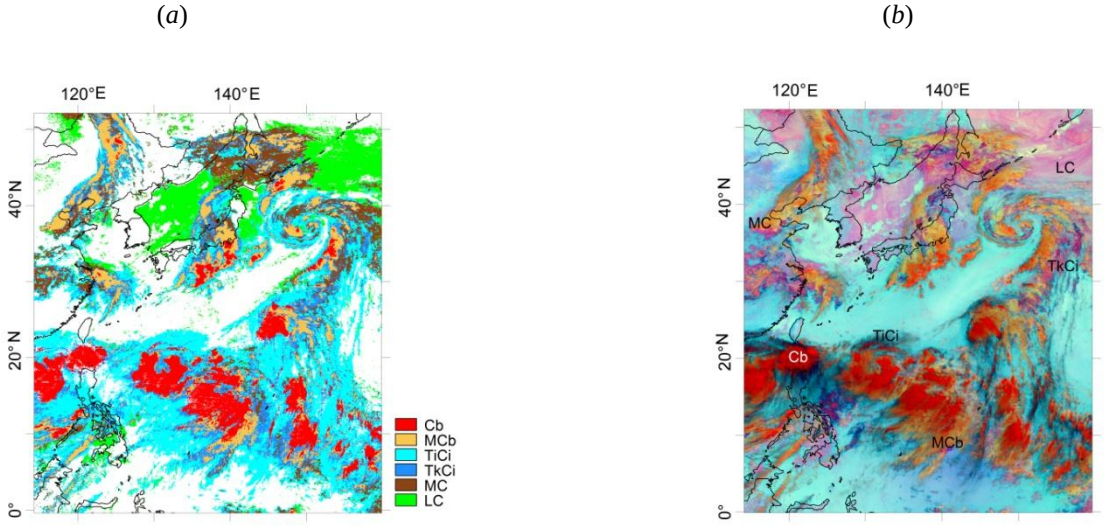

Figure 3. (*a*) Cloud-type classification result obtained using 2D-THR algorithm and (*b*) its corresponding night-time microphysical colour composite for 2 August 2009 at 02:30 UTC.

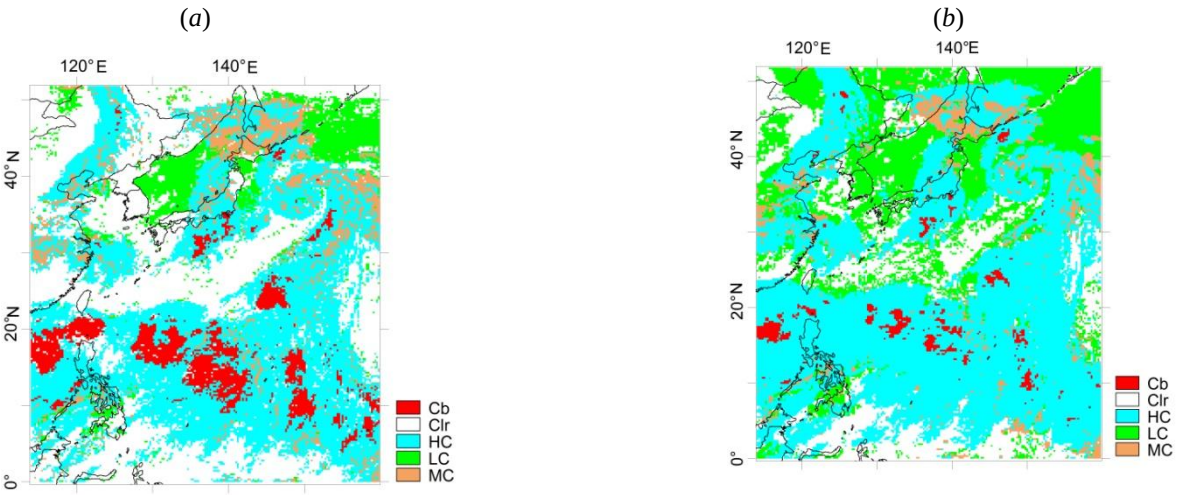

Figure 4. Inter-comparison of the reclassified cloud type classification between (*a*) 2D-THR cloud type classification result and (*b*) the JMA product for 2 August 2009 02:30 UTC. 2D-THR is resampled into the same spatial resolution as JMA.

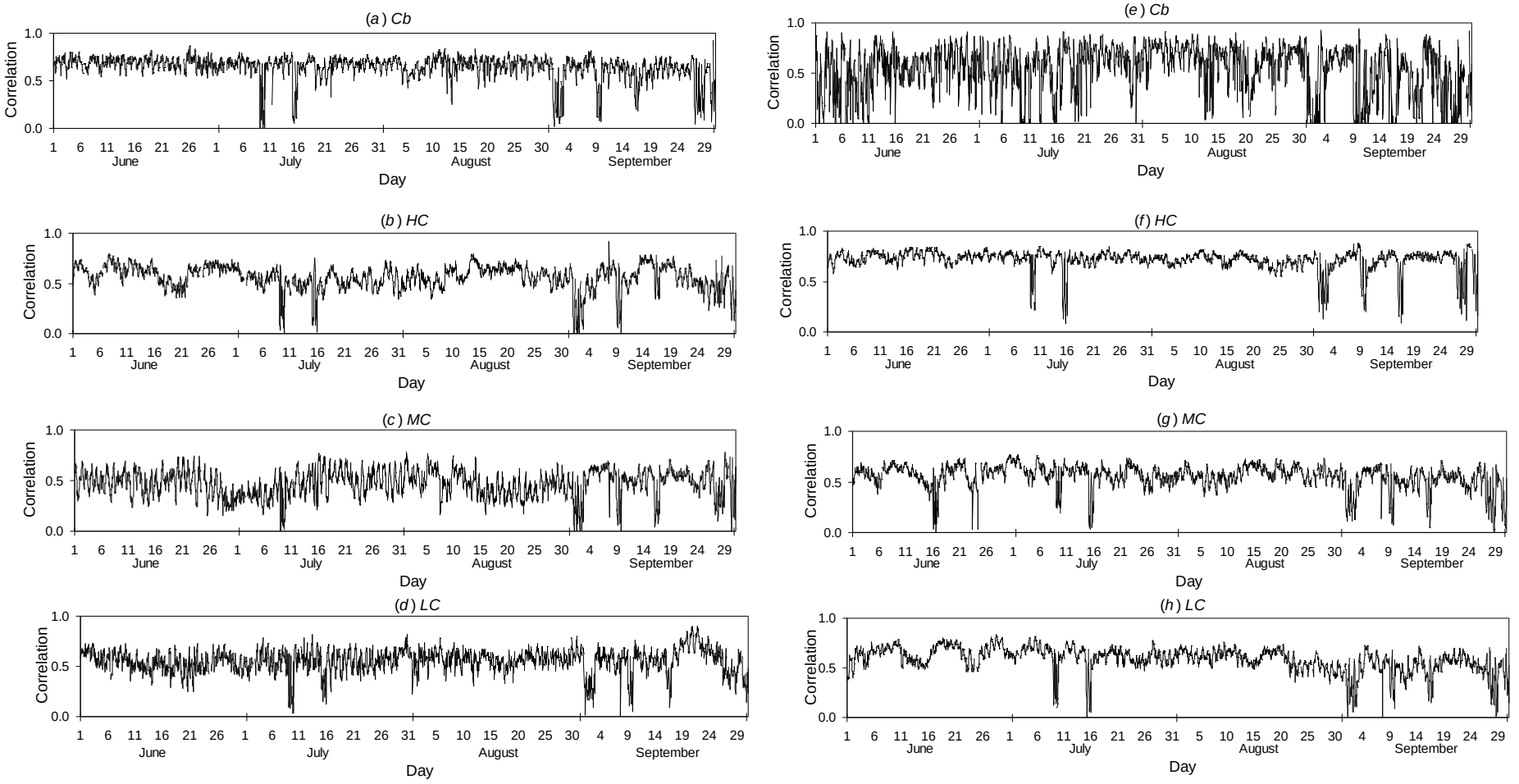

Figure 5. Hourly variation in the spatial correlation of Cb ((*a*) and (*e*)), HC ((*b*) and (*f*)), MC ((*c*) and (*g*)) and LC ((*d*) and (*h*)) percentage between 2D-THR and JMA cloud classification for tropical region ((*a*)–(*d*)) and subtropical region ((*e*)–(*h*)) during June, July, August and September 2009.